VOLUMETRIC SEGMENTATION OF MULTIPLE BASAL GANGLIA STRUCTURES USING NONPARAMETRIC COUPLED SHAPE AND INTER-SHAPE POSE PRIORS

Mustafa Gökhan Uzunbaş, Octavian Soldea, Müjdat Çetin, Gözde Ünal, Aytül Erçil *

Faculty of Engineering and Natural Sciences, Sabanci University, Tuzla, 34956 İstanbul, Turkey

Devrim Unay, Ahmet Ekin

The Video Processing and Analysis Group,
Philips Research Europe,
Eindhoven, The Netherlands

Zeynep Firat

The Radiology Department of the
Yeditepe University Hospital,
Istanbul, Turkey

ABSTRACT

We present a new active contour-based, statistical method for simultaneous volumetric segmentation of multiple subcortical structures in the brain. Neighboring anatomical structures in the human brain exhibit co-dependencies which can aid in segmentation, if properly analyzed and modeled. Motivated by this observation, we formulate the segmentation problem as a maximum *a posteriori* estimation problem, in which we incorporate statistical prior models on the shapes and inter-shape (relative) poses of the structures of interest. This provides a principled mechanism to bring high level information about the shapes and the relationships of anatomical structures into the segmentation problem. For learning the prior densities based on training data, we use a nonparametric multivariate kernel density estimation framework. We combine these priors with data in a variational framework, and develop an active contour-based iterative segmentation algorithm. We test our method on the problem of volumetric segmentation of basal ganglia structures in magnetic resonance (MR) images and present a quantitative performance analysis. We compare our technique with existing methods and demonstrate the improvements it provides in terms of segmentation accuracy.

***Index Terms*—** Volumetric segmentation, active contours, shape prior, kernel density estimation, moments, MR imagery, basal ganglia.

1. INTRODUCTION

Segmentation of subcortical structures in brain magnetic resonance (MR) images is motivated by a number of medical objectives including the early diagnosis of neurodegenerative illnesses such as schizophrenia, Parkinson's, and Alzheimer's diseases [1]. Segmentation of subcortical brain structures, such as the caudate nucleus and the putamen, is a challenging task due to a number of factors including the low intensity contrast in MR images. Due to such data quality limitations, purely data-driven approaches do not usually achieve satisfactory segmentation performance. This motivates the use of prior information at various levels. In particular, statistical information about the shapes of the structures, as well as relationships between these anatomical structures, such as relative (inter-shape) pose could prove to be valuable.

Variational techniques provide a principled framework for formulating segmentation problems [2, 3], and have been widely used with biomedical data. One approach used in the solution of such problems involves active contour or curve evolution techniques. In recent active contour models, there has been an increasing interest in using prior models for the shapes to be segmented (see e.g. [4, 5, 6, 7, 8]). While earlier approaches [4] can be used towards segmentation employing unimodal Gaussian-like shape densities, more recent techniques [5, 6, 7, 8] capture nonlinear shape variability and multi-modal probability density functions for shapes.

While the techniques mentioned above could be used to introduce prior information on the shapes of multiple objects independently, another piece of information that could be useful involves dependencies both between the shapes of the multiple structures as well as between the poses (location, size, orientation) of the structures of interest. Such dependencies are modeled and used, for example, in [9, 10, 11, 12, 13]. In this paper, we take a different approach, and introduce statistical joint prior models of multiple-structures into an active contour segmentation method in a nonparametric multivariate kernel density estimation framework. In our previous work [14], we introduced prior probability densities on the coupled (joint) shapes of the structures of interest for 2D segmentation. In this paper, we propose a framework which includes not only coupled shape priors, but also inter-shape (relative) pose priors for the multiple structures to be segmented, and apply this technique to 3D data. We use multivariate Parzen density estimation to estimate the unknown joint density of multiple object shapes, as well as inter-shape poses, based on expert-segmented training data. For inter-shape pose representation, we use standard moments, which are intrinsic to shape and have natural physical interpretations [15]. Given these learned prior densities, we pose the segmentation problem as a maximum *a posteriori* estimation problem combining the prior densities with data. We derive gradient flow expressions for the resulting optimization problem, and solve the problem using active contours. To the best of our knowledge, our approach is the first scheme of multi-object segmentation employing coupled nonparametric shape and inter-shape pose priors. We demonstrate the effectiveness of this approach on volumetric segmentations in real MR images accompanied by a quanti-

*This work was partially supported by the European Commission under Grants MTKI-CT-2006-042717 (IRonDB), FP6-2004-ACC-SSA-2 (SPICE), MIRG-CT-2006-041919, and a graduate fellowship from The Scientific and Technological Research Council of Turkey (TUBITAK). The MR brain data sets were provided by the Radiology Center at Yeditepe University Hospital.

tative analysis of the segmentation accuracy.

2. SEGMENTATION USING COUPLED PRIORS

We define an energy (cost) functional in a MAP estimation framework as

$$E(\mathbf{C}) = -\log P(data|\mathbf{C}) - \log P(\mathbf{C}), \quad (1)$$

where $\mathbf{C}$ is a set of evolving contours $\left\{C^1, ..., C^m\right\}$ that represent the boundaries of m different anatomical structures (e.g. caudate nucleus, putamen, etc.). In the following, we will refer to [2] as $C\&V$. We choose the likelihood term $P(data|\mathbf{C})$ as in $C\&V$. In this work, we focus on building $P(\mathbf{C})$, which is a coupled prior density of multiple structures (or objects).

The geometric information in $\mathbf{C}$ consists of shape $\widetilde{\mathbf{C}}$ and pose $\mathbf{p}$, i.e. $P(\mathbf{C}) = P(\widetilde{\mathbf{C}}, \mathbf{p})$, where $\mathbf{p}$ is a vector of pose parameters (location, size, orientation) for each structure, and $\widetilde{\mathbf{C}} = T[\mathbf{p}]\mathbf{C}$ denotes the aligned version of the boundaries (i.e. $T[\mathbf{p}]$ is an alignment operator that brings the curves to some reference pose). We decompose the pose $\mathbf{p}$ into a global pose p_{glb} of the ensemble of structures, and inter-shape poses $\mathbf{p}_{int} = (p^1_{int}, ..., p^m_{int})$ of each structure, i.e. $\mathbf{p} = (p_{glb}, \mathbf{p}_{int})$. When the structures are globally aligned, the remaining variability in the pose of individual structures is captured by $\mathbf{p}_{int}$. Given these definitions, we have

$$P(\mathbf{C}) = P\left(p_{glb}, \mathbf{p}_{int}|\widetilde{\mathbf{C}}\right) \cdot P\left(\widetilde{\mathbf{C}}\right). \quad (2)$$

Conditioned on $\widetilde{\mathbf{C}}$, we model p_{glb} and $\mathbf{p}_{int}$ as independent variables, because the global pose of the structures and inter-shape poses are not expected to provide information about each other. In addition, $P(p_{glb}|\widetilde{\mathbf{C}})$ is assumed to be uniform since all poses p_{glb} are equally likely.[1] Then (2) becomes

$$P(\mathbf{C}) = P\left(\mathbf{p}_{int}|\widetilde{\mathbf{C}}\right) \cdot \gamma \cdot P\left(\widetilde{\mathbf{C}}\right),$$

where γ is a normalizing scalar. In this context, the coupled shape density $P(\widetilde{\mathbf{C}})$ disregards all the pose variability and focuses only on shape variability, whereas $P(\mathbf{p}_{int}|\widetilde{\mathbf{C}})$ provides a density on the relative pose of shapes. The inter-shape pose prior is estimated over globally aligned multiple object contours while the shape prior is estimated over both globally and locally aligned ones. Considering this key point, let $\bar{\mathbf{C}} = (\mathbf{p}_{int}, \widetilde{\mathbf{C}})$ denote the globally aligned multiple object contours, (see Figure1) . We can then represent the inter-shape pose prior in terms of the curves which encompass internal pose variation, conditioned on the shapes whose global and local pose variation is removed. Then the overall prior can be written as:

$$P(\mathbf{C}) = P\left(\bar{\mathbf{C}}|\widetilde{\mathbf{C}}\right) \cdot \gamma \cdot P\left(\widetilde{\mathbf{C}}\right).$$

Using these definitions, (1) can be expressed as

$$E(\mathbf{C}) \propto -\log P(data|\mathbf{C}) - \log P\left(\bar{\mathbf{C}}|\widetilde{\mathbf{C}}\right) - \log P\left(\widetilde{\mathbf{C}}\right). \quad (3)$$

Segmentation is achieved by finding the set of curves $\mathbf{C}$ that minimize (3) through active contour-based gradient flow.

[1] In some applications where certain global poses are more likely *a priori*, a non-uniform density could be used.

2.1. Coupled Shape Prior for Multiple Structures

In this subsection we discuss the learning and use of $P(\widetilde{\mathbf{C}})$. We have N training samples, where each sample consists of expert-segmented multiple structures. We estimate the joint shape density $P(\widetilde{\mathbf{C}})$ through kernel density estimation:

$$P\left(\widetilde{\mathbf{C}}\right) = \frac{1}{N}\sum_{i=1}^{N}\prod_{j=1}^{m} k(d(\phi_{\widetilde{C}^j}, \phi_{\widetilde{C}^j_i}), \sigma_j). \quad (4)$$

We can then evaluate this density for any curve ensemble $\widetilde{\mathbf{C}}$. Here $k(., \sigma)$ is a Gaussian kernel with standard deviation σ, ϕ_C denotes the signed distance function of contour C, the index j refers to the j^{th} structure in the multi-structure ensemble, and i points to the i^{th} training sample. Finally, $d(\cdot, \cdot)$ is a distance metric, and we use the Euclidean distance [7]. Given this learned density, its contribution to the gradient flow for (3) is given by (expressed for $m = 2$ for simplicity):

$$\frac{\partial \phi_{\widetilde{C}^j}}{\partial t} = \frac{1}{\sigma_j^2}\sum_{i=1}^{N}\lambda_i(\widetilde{C}^1, \widetilde{C}^2)(\phi_{\widetilde{C}^j_i}(x,y) - \phi_{\widetilde{C}^j}(x,y)) \quad (5)$$

where $j = 1, 2$, $\lambda_i\left(\widetilde{C}^1, \widetilde{C}^2\right) = \frac{k^1_i k^2_i}{N \cdot P\left(\widetilde{C}^1, \widetilde{C}^2\right)}$, and $k^j_i = k\left(d\left(\phi_{\widetilde{C}^j}, \phi_{\widetilde{C}^j_i}\right), \sigma_j\right)$. Note that training shapes that are closer to the evolving contour influence the evolution with higher weights. Note also that the weighting function $\lambda_i(\widetilde{C}^1, \widetilde{C}^2)$ exhibits the coupling between the multiple structures.

2.2. Relative Pose Prior for Multiple Structures

In this subsection we discuss the learning and use of $P(\bar{\mathbf{C}}|\widetilde{\mathbf{C}})$. We estimate $P(\bar{\mathbf{C}}|\widetilde{\mathbf{C}})$ through kernel density estimation as follows:

$$P(\bar{\mathbf{C}}|\widetilde{\mathbf{C}}) = \frac{1}{N}\sum_{i=1}^{N}\prod_{j=1}^{m} k\left(d\left(p^j_{int}, p^{ji}_{int}\right), \sigma_j\right), \quad (6)$$

where p^{ji}_{int} is the relative pose of the i^{th} element of the j^{th} structure in the training set, whereas p^j_{int} is the relative pose of the j^{th} structure in the candidate curve ensemble. Here $d(\cdot, \cdot)$ is a weighted Euclidean distance. In 2D (for notational simplicity and without loss of generality), the relative pose of each structure is given by $p_{int} = [A, c_x, c_y, \theta]$.[2] Here, A is the area, c_x and c_y are the coordinates of the structure, and θ is the orientation of the structure, all computed after global alignment.

We use moments to compute the relative poses: $p_{int} = \left[m_{0,0}, \frac{m_{1,0}}{m_{0,0}}, \frac{m_{0,1}}{m_{0,0}}, \theta\right]$. Here, $m_{0,0}$ represents area, $\frac{m_{1,0}}{m_{0,0}}, \frac{m_{0,1}}{m_{0,0}}$ are horizontal and vertical positions relative to the mass center, and θ is the orientation. Following [15], the two-dimensional moment, m, of order $p+q$, on a signed distance function ϕ, is computed as: $m_{p,q} = \int_{x=-\infty}^{\infty}\int_{y=-\infty}^{\infty} x^p y^q H(-\phi(x,y))\, dxdy$, where H is the heaviside function. The orientation of contour C is defined as [15]

$$\theta(C) = \frac{1}{2}\arctan\left(\frac{2\left(m_{1,0}m_{0,1} - m_{1,1}m_{0,0}\right)}{\left(m_{0,2} - m_{2,0}\right)m_{0,0} + m^2_{1,0} - m^2_{0,1}}\right)$$

Let $k^j_i = k(d(p^j_{int}, p^{ji}_{int}), \sigma_j)$. Then, the gradient flow for (6) is

$$\frac{\partial \phi_{\bar{C}^j}}{\partial t} = \frac{1}{P(\bar{\mathbf{C}}|\widetilde{\mathbf{C}}) \cdot N}\sum_{i=1}^{N}\left(\prod_{j=1}^{m} k^j_i\right)\frac{MPF(j,i)}{{\sigma_j}^2}\delta_\epsilon(\phi_{\bar{C}^j}), \quad (7)$$

[2] We drop indices for simplicity.

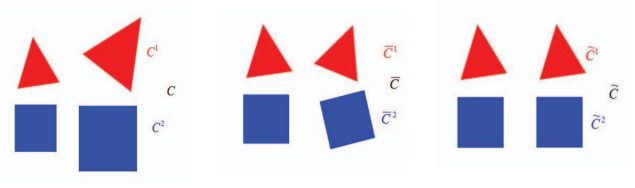

(a) (b) (c)

Fig. 1. Alignment terms used for a multi-object that consists of a red triangle and a blue square. In each figure, the left side multi-object is a reference to which the right multi-object is aligned to. In Figure (a), the multi-object C is unaligned. In Figure (b), $\overline{C}$ is aligned globally. In Figure (c), $\widetilde{C}$ is aligned locally, i.e. each (sub)object is aligned separately. In Figures (b) and (c), the multi-objects are not superimposed due to illustration reasons.

where

$$
\begin{aligned}
MPF(j,i) \quad = \quad & \left(m^{j}_{0,0} - {m_{0,0}}^{ji}\right) \\
& + \sum_{(r,s),r+s=1} \left(\frac{m^{j}_{r,s}}{m^{j}_{0,0}} - \frac{{m_{r,s}}^{ji}}{{m_{0,0}}^{ji}} \right) \frac{\left(x^r y^s m^{j}_{0,0} - m^{j}_{r,s}\right)}{\left(m^{j}_{0,0}\right)^2} \\
& + \left(\theta^j - \theta^{ji}\right) \sum_{r=0}^{2} \sum_{s=0}^{2-r} x^r y^s M^{\theta j}_{rs}
\end{aligned} \tag{8}
$$

for each $j \in \{1, \cdots, m\}$. In implementation, we employ δ_ϵ, which is a smooth approximation to δ [2]. Here, $m^{j}_{r,s}$ and $m^{ji}_{r,s}$ denote the moments of $\bar{C}^j$ and $\bar{C}^j_i$, respectively, and the angles θ follow the same convention. Due to space limitations, we are not able to provide details about the term $M^{\theta j}_{r,s}$, which can be found in [16].

Note that in order to specify the kernel size σ_j of the jth object, we use the maximum likelihood kernel size with leave-one-out method (see [17]). This choice is used both in Sections 2.1 and 2.2.

Overall, the contributions from the C&V data term [2], coupled shape prior (Eqn. (5)), and the inter-shape pose prior (Eqn. (7)) constitute the gradient flow for (3). These three forces are summed at each iteration of the segmentation process, after appropriate alignment operations [16].

3. EXPERIMENTAL RESULTS

We present 3D experimental results for the head of caudate nucleus and putamen. Our data set consists of seven registered T2 MR images. Our ground truths are binary volumes segmented by medical operators from these MR images. We select one image for testing and we use the rest of six for training. We compare the segmentation results of our proposed approach with those of C&V in Figures 2, 3 and 4. Overall, we observe that C&V results in serious leakages in both structures, whereas our approach produces boundaries visually much closer to the ground truths. This qualitative observation is confirmed by the quantitative performance results in Table 1. In particular, in terms of the Dice error rate $1 - DC$ [18], our approach provides significant improvements over C&V. Note that we compute the Dice coeficients between segmentation results and ground truth. Our scheme requires about one hundred seconds to reach the steady state for each 200x200x50 voxel volume, using the level set framework of ITK (see http://www.itk.org).

4. CONCLUSION

We have presented a multi-object segmentation approach that employs nonparametric coupled shape and inter-shape pose priors for different basal ganglia structures. We employ an active contour framework towards evolving different contours in parallel. The priors are learned using kernel density estimation. We have demonstrated our approach in several experiments, in which poorly contrasted shapes are successfully segmented. In addition, quantitative performance analysis and comparisons to well-established techniques are presented.

Currently, we are working on applying our approach on other subcortical structures than the caudate nucleus and the putamen. We also plan to compare our approach to other segmentation techniques involving shape priors. In addition, we intend to introduce a more structured data term, based on intensity characteristics of the tissues.

	1 - DC
C&V	0.268
Proposed Approach	0.2335

Table 1. Quantitative accuracy results.

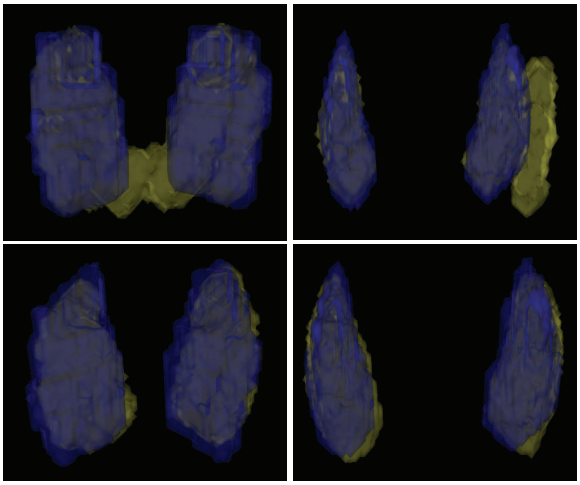

Fig. 2. A comparison of segmentation results to ground truths. Left: caudate nucleus; right: putamen. Blue: ground truth; yellow: segmentation result by C&V (top) and proposed approach (bottom).

5. REFERENCES

[1] E. Madsen and J. D. Gitlin, "Copper and iron disorders of the brain," *Annual Review of Neuroscience*, vol. 30, pp. 317–337, March 2007.

[2] T. F. Chan and L. A. Vese, "Active contours without edges," *IEEE Transactions on Image Processing*, vol. 10, no. 2, pp. 266–277, 2001.

[3] A. Tsai, A. J. Yezzi, and A. S. Willsky, "A curve evolution approach to medical image magnification via the Mumford-Shah functional," *Medical Image Computing and Computer-Assisted Intervention, Lecture Notes in Computer Science*, vol. 1935, pp. 246–255, 2000.

[4] A. Tsai, A. Yezzi Jr., W. Wells, C. Tempany, D. Tucker, A. Fan, W. E. Grimson, and A. Willsky, "A shape-based approach to the segmentation of medical imagery using level sets," *IEEE*

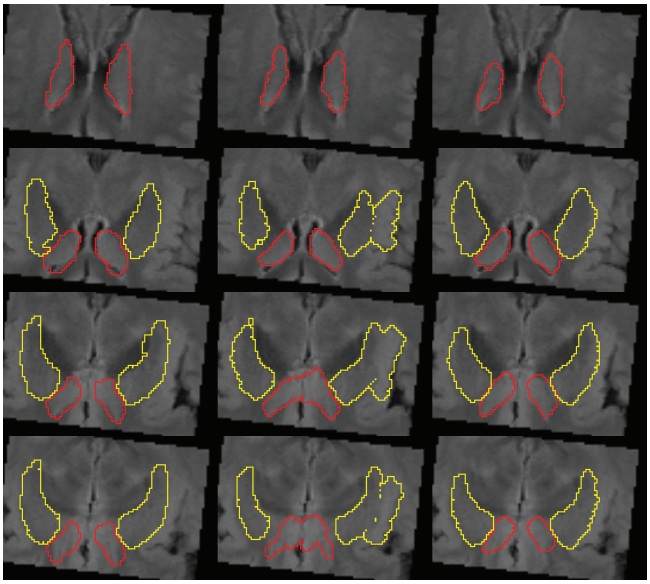

Fig. 3. A comparison on 2D axial slices from 3D segmentations. Red: caudate nucleus; yellow: putamen. Left: ground truth; middle column: C&V; right: proposed approach. Each row corresponds to a different slice.

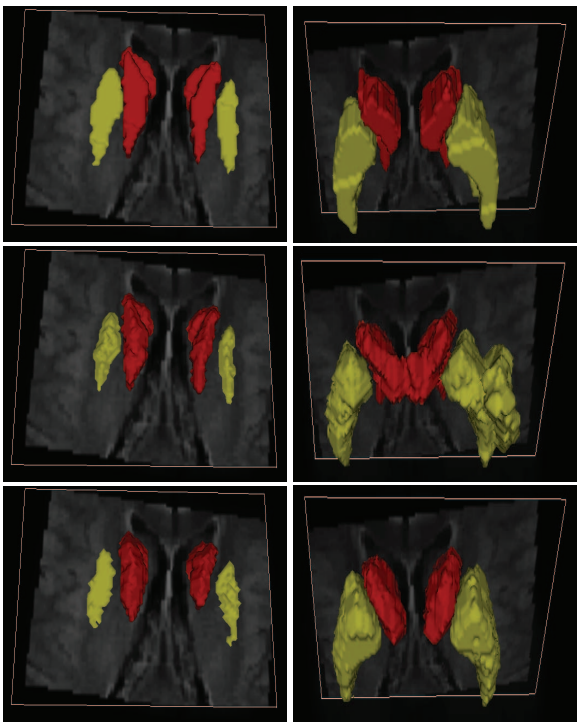

Fig. 4. Comparison of volumetric segmentations from two viewpoints (left and right columns). Red: caudate nucleus; yellow: putamen. Top: ground truth; middle row: C&V; bottom: proposed approach.

Transactions on Medical Imaging, vol. 22, no. 2, pp. 137–154, February 2003.

[5] D. Cremers, S. J. Osher, and S. Soatto, "Kernel density estimation and intrinsic alignment for shape priors in level set segmentation," *International Journal of Computer Vision*, vol. 69, no. 3, pp. 335–351, 2006.

[6] S. Dambreville, Y. Rathi, and A. Tannenbaum, "A framework for image segmentation using shape models and kernel space shape priors," *IEEE Transactions on Pattern Analysis and Machine Intelligence*, vol. 30, no. 8, pp. 1385–1399, 2008.

[7] J. Kim, M. Çetin, and A. S. Willsky, "Nonparametric shape priors for active contour-based image segmentation," *Signal Processing*, vol. 87, no. 12, pp. 3021–3044, December 2007.

[8] K. Gorczowski, M. Styner, J. Y. Jeong, J. S. Marron, J. Piven, H. C. Hazlett, S. M. Pizer, and G. Gerig, "Discrimination analysis using multi-object statistics of shape and pose," *Society of Photo-Optical Instrumentation Engineers (SPIE) Conference Series, Medical Imaging: Image Processing*, vol. 6512, March 2007.

[9] A. Tsai, W. Wells, C. Tempany, E. Grimson, and A. Willsky, "Mutual information in coupled multi-shape model for medical image segmentation," *Medical Image Analysis*, vol. 8, no. 4, pp. 429–445, 2004.

[10] J. Yang, L. H. Staib, and J. S. Duncan, "Neighbor-constrained segmentation with level set based 3D deformable models," *IEEE Transactions on Medical Imaging*, vol. 23, no. 8, pp. 940–948, August 2004.

[11] A. Litvin and W. C. Karl, "Coupled shape distribution-based segmentation of multiple objects," *Information Processing in Medical Imaging, Lecture notes In Computer Science*, vol. 3565, pp. 345–356, 2005.

[12] M. Rousson and C. Xu, "A general framework for image segmentation using ordered spatial dependency," *Medical Image Computing and Computer-Assisted Intervention, Lecture Notes in Computer Science*, vol. 4191, pp. 848–855, 2006.

[13] M. Styner, K. Gorczowski, T. Fletcher, J. Y. Jeong, S. M. Pizer, and G. Gerig, "Statistics of pose and shape in multi-object complexes using principal geodesic analysis," *International Workshop on Medical Imaging and Augmented Reality, Lecture Notes in Computer Science*, vol. 4091, pp. 1–8, 2006.

[14] G. Uzunbaş, M. Çetin, G. Ünal, and A. Erçil, "Coupled nonparametric shape priors for segmentation of multiple basal ganglia structures," *The Fifth IEEE International Symposium on Biomedical Imaging: From Nano to Macro, ISBI 2008.*, pp. 217–220, 2008.

[15] R. J. Prokop and A. P. Reeves, "A survey of moment-based techniques for unoccluded object representation and recognition," *CVGIP: Graphical Models and Image Processing*, vol. 54, no. 5, pp. 438–460, September 1992.

[16] M. G. Uzunbaş, "Segmentation of multiple brain structures using coupled nonparametric shape priors," *M. Sc. Thesis, Sabanci University*, 2008.

[17] B. W. Silverman, *Density Estimation for Statistics and Data Analysis*, Chapman Hall/CRC, London, 1986.

[18] L. R. Dice, "Measures of the amount of ecologic association between species," *Ecology*, vol. 26, no. 3, pp. 297–302, July 1945.